physica status solidi b
www.pss-b.com

Acoustic Phonon Scattering in Free-Standing Anisotropic Silicon Plates

Nobuya Mori

The electron–acoustic-phonon interaction in a free-standing anisotropic Si plate with (001) surface is studied taking into account the elastic anisotropy of the Si crystal and the modulated phonon modes. The interaction potential is derived from the modulated phonon modes and the anisotropic deformation potential constants. The effective deformation potential constant D_{ac} is then calculated considering only the lowest electronic sub-band. In the quantum well model for the electronic states, it is shown that the effective deformation potential for the modulated phonons in an anisotropic Si plate becomes $D_{ac} \approx 13$ eV in the thinner region of the plate thickness $w \lesssim 3.2$ nm. It is also shown that both the phonon modulation and the crystal anisotropy have non-negligible effects on the effective deformation potential and electron mobility.

1. Introduction

Continuous technological innovation in the semiconductor industry has made it possible to produce Si metal–oxide–semiconductor field-effect transistors (MOSFETs) with channel lengths of less than a few tens of nanometers.[1–7] In order to suppress the short-channel effects in such ultrasmall devices, it is necessary to introduce ultrathin channels on the nanometer scale.[8] Since one of the major factors limiting the electron mobility in Si MOSFETs is the intravalley acoustic phonon scattering,[9–15] it is important to perform a detailed analysis of the electron–acoustic-phonon interaction in ultrathin channels for the design of the ultrasmall MOSFETs.

In a semiconductor plate, not only the electronic states but also the acoustic phonon modes are modulated. The electron–phonon interaction is thus generally different from that assumed for phonon modes in the bulk. Ezawa et al. introduced "surfons," the quanta of elastic waves in solids that have a boundary surface or phonons in a half-space. Based on the surfons, they analyzed the electron mobility of two-dimensional electron gas (2DEG) in planar Si MOSFETs.[16–20] Bannov et al. studied confined acoustic phonons in a free-standing semiconductor plate and their interaction with electrons.[21–23] Donetti et al. developed a model for confined acoustic phonons in three-layer systems and analyzed the electron mobility in silicon-on-insulator (SOI) structures.[24,25] Uno et al. considered modulated acoustic phonons in a free-standing semiconductor plate. It was shown that the form factors for electron–modulated-acoustic-phonon interaction satisfy sum rules and lie on a universal curve regardless of plate thickness and material.[26–29] These studies, however, assume that the semiconductor crystal is an isotropic elastic body, and the effect of the elastic anisotropy of the crystal has not been clarified yet. The crystal anisotropy leads to the anisotropic deformation potential constants and the anisotropic phonon dispersions. As a result, the strength of electron scattering by acoustic phonons may be different from that assumed in an isotropic model. In order to accurately predict electron mobility and other transport properties in Si-confined structures, it is important to study how the anisotropy of the crystal affects the transport properties.

The intravalley electron–acoustic-phonon interaction is characterized by a two-rank deformation-potential tensor, Ξ_{ij}. For the Δ valleys in the Si conduction band, Ξ_{ij} can be expressed in terms of the dialational and shear deformation potential constants (Ξ_d and Ξ_u);[30] the interaction strength depends on the direction of the phonon wavevector. For device modeling and simulation, however, this anisotropy of the deformation potential is often neglected. An isotropic acoustic phonon approximation is then used by introducing an effective deformation potential constant D_{ac}.[10,13,31] It is the key parameter that effectively describes the strength of electron–acoustic-phonon scattering and has been widely used in device modeling because it gives us a convenient way to estimate electron mobility with a single number. The effective deformation potential constant $D_{ac} = 9$ eV is known for bulk Si.[10,32,33] For a Si MOS inversion layer, however, it has been reported that higher values are required to explain the experimental mobilities,[34–37] such as $D_{ac} = 12$[34,37] and 12.9 eV.[35] For SOI MOSFETs, it has been reported that D_{ac} increases sharply at the MOS interfaces; the effective deformation potential varies from $D_{ac} = 10.5$–18 eV with the characteristic length of ≈3 nm.[38] Although the detailed mechanism behind this sharp increase in D_{ac} was not elucidated in ref. [38], the results have strong implications for accurate device modeling in the design of high-performance and/or low-power MOSFETs.

N. Mori
Division of Electrical, Electronic and Infocommunications Engineering
Osaka University
Suita, Osaka 565–0871, Japan
E-mail: nobuya.mori@eei.eng.osaka-u.ac.jp

The ORCID identification number(s) for the author(s) of this article can be found under https://doi.org/10.1002/pssb.202400540.

DOI: 10.1002/pssb.202400540

In this paper, we study the electron–acoustic-phonon interaction in a free-standing Si plate with (001) surface. In particular, we try to clarify the role of the modulated phonons on the electron–acoustic-phonon interaction considering the elastic anisotropy of the Si crystal and the anisotropy of the deformation potential. We proceed as follows. First, we obtain the modulated phonon modes taking into account the elastic anisotropy by the method of Solie and Auld.[39] These phonon modes allow us to derive the electron–acoustic-phonon interaction Hamiltonian with the anisotropic deformation potential constants. We then calculate the momentum relaxation time considering only the lowest electronic sub-band and evaluate the acoustic-phonon-limited electron mobility. Finally, the electron mobility is converted to the effective deformation potential constant $D_{\rm ac}$ for comparison with the previous studies.

The organization of the present paper is as follows. In Section 2, we derive the modulated phonon modes taking into account the elastic anisotropy. Although the method follows Solie and Auld,[39] we describe it for the sake of completeness and to introduce the notations. We then derive the electron–acoustic-phonon interaction potential and show the formalism for the momentum relaxation time and the acoustic-phonon-limited electron mobility. In Section 3, we present the calculated results of the phonon dispersion and the effective deformation potential and discuss the effect of the anisotropies on the electron–acoustic-phonon interaction in a Si plate. A conclusion is given in Section 4.

2. Theory

2.1. Phonon Modes

We consider a free-standing Si plate with (001) surface and thickness w whose geometry is given in **Figure 1**a. The surface is normal to the z-axis and the plate occupies $-w/2 \le z \le w/2$. Let us consider a partial wave of the lattice displacement vector $\boldsymbol{u}$ $(= (u_x, u_y, u_z))$ of the form[39]

$$\boldsymbol{u} = \boldsymbol{\alpha} \exp\left[i(q_x x + q_y y + q_z z)\right] \tag{1}$$

Here, $\boldsymbol{\alpha} = (\alpha_x, \alpha_y, \alpha_z)$ represents the direction and the amplitude of the displacement. The lattice displacement vector satisfies the Christoffel equation

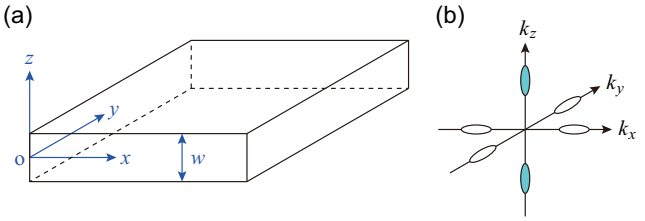

Figure 1. a) Anisotropic Si plate with a (001) surface lying between $z = \pm\frac{1}{2}w$ with the surface normal to the z-axis. The crystal axes [100] and [010] coincide with the x and y axes, respectively. b) Schematic constant-energy surface for the conduction band of Si in the momentum space, showing six valleys with the longitudinal effective mass m_ℓ and the transverse effective mass $m_{\rm t}$.

$$(q_{iI} c_{IJ} q_{Jj} - \rho\omega^2 \delta_{ij}) u_j = 0 \tag{2}$$

Here, the following subscript notation is used[40,41]

$$i, j = x, \quad y, \quad z \tag{3}$$

$$I, J = \begin{matrix} xx, & yy, & zz, & yz, & zx, & xy \\ 1 & 2 & 3 & 4 & 5 & 6 \end{matrix} \tag{4}$$

and summation over repeated subscripts is assumed. In Equation (2), ρ is the mass density, ω is the vibrational frequency, c_{IJ} is the elastic stiffness constant, the matrix q_{iI} is

$$q_{iI} = \begin{bmatrix} q_x & 0 & 0 & 0 & q_z & q_y \\ 0 & q_y & 0 & q_z & 0 & q_x \\ 0 & 0 & q_z & q_y & q_x & 0 \end{bmatrix} \tag{5}$$

and q_{Jj} is the transpose. Since Si belongs to the cubic crystal system, c_{IJ} have three independent components, c_{11}, c_{12}, and c_{44}.[40] The elastic anisotropy of the crystal can be measured by the quantity $c^* = c_{11} - c_{12} - 2c_{44}$.[30]

Considering a mode whose 2D in-plane wavevector is given by $\boldsymbol{q} = q(\cos\phi, \sin\phi) = q(\ell_x, \ell_y)$ with ϕ being the angle between $\boldsymbol{q}$ and the x-axis, Equation (2) is reduced to

$$D\boldsymbol{\alpha} = 0 \tag{6}$$

where the 3×3 matrix D is defined by

$$D = \begin{bmatrix} d_{xx} - \rho v^2 & d_{xy} & d_{xz} \\ d_{yx} & d_{yy} - \rho v^2 & d_{yz} \\ d_{zx} & d_{zy} & d_{zz} - \rho v^2 \end{bmatrix} \tag{7}$$

$v = \omega/q$ is the phase velocity, $\ell_z = q_z/q$, and d_{ij} are given by

$$d_{ii} = (c_{12} + c_{44} + c^*)\ell_i^2 + c_{44}(\ell_z^2 + 1) \tag{8}$$

$$d_{ij} = (c_{12} + c_{44})\ell_i \ell_j, \quad (i \ne j) \tag{9}$$

Nontrivial solutions to Equation (6) exist only when the determinant $|D|$ vanishes. The equation $|D| = 0$ is a third-order polynomial in $(\ell_z)^2$ (or a sixth-order polynomial in ℓ_z) with the three roots in $(\ell_z)^2$

$$\left(L_z^{(k)}\right)^2, \quad k = 1, 2, 3 \tag{10}$$

Using these $L_z^{(k)}$ $(k = 1, 2, 3)$, the six roots in ℓ_z can be written as

$$\begin{aligned} &\left(\ell_z^{(1)}, \ell_z^{(2)}, \ell_z^{(3)}, \ell_z^{(4)}, \ell_z^{(5)}, \ell_z^{(6)}\right) \\ &= \left(L_z^{(1)}, L_z^{(2)}, L_z^{(3)}, -L_z^{(1)}, -L_z^{(2)}, -L_z^{(3)}\right) \end{aligned} \tag{11}$$

Denoting the corresponding $\boldsymbol{\alpha}$ to $\ell_z^{(k)}$ as $\boldsymbol{\alpha}^{(k)}$ $(k = 1, 2, \ldots, 6)$, we have

$$\begin{aligned} &\left(\alpha_j^{(1)}, \alpha_j^{(2)}, \alpha_j^{(3)}, \alpha_j^{(4)}, \alpha_j^{(5)}, \alpha_j^{(6)}\right) \\ &= \left(\alpha_j^{(1)}, \alpha_j^{(2)}, \alpha_j^{(3)}, \alpha_j^{(1)}, \alpha_j^{(2)}, \alpha_j^{(3)}\right), \quad (j = x, y) \end{aligned} \tag{12}$$

$$\left(\alpha_z^{(1)}, \alpha_z^{(2)}, \alpha_z^{(3)}, \alpha_z^{(4)}, \alpha_z^{(5)}, \alpha_z^{(6)}\right) = \left(\alpha_z^{(1)}, \alpha_z^{(2)}, \alpha_z^{(3)}, -\alpha_z^{(1)}, -\alpha_z^{(2)}, -\alpha_z^{(3)}\right) \tag{13}$$

The general solution $\boldsymbol{u}$ to Equation (2) is then written as

$$u_j = \sum_{k=1}^{6} C_k \alpha_j^{(k)} \exp\left[iq\left(x\ell_x + y\ell_y + z\ell_z^{(k)}\right)\right] = \sum_{k=1}^{3} \alpha_j^{(k)} e^{i\boldsymbol{q}\cdot\boldsymbol{x}}\left[S_k \cos\left(qL_z^{(k)}z\right) + iA_k \sin\left(qL_z^{(k)}z\right)\right], \quad (j = x, y) \tag{14}$$

$$u_z = \sum_{k=1}^{6} C_k \alpha_z^{(k)} \exp\left[iq\left(x\ell_x + y\ell_y + z\ell_z^{(k)}\right)\right] = \sum_{k=1}^{3} \alpha_z^{(k)} e^{i\boldsymbol{q}\cdot\boldsymbol{x}}\left[iS_k \sin\left(qL_z^{(k)}z\right) + A_k \cos\left(qL_z^{(k)}z\right)\right] \tag{15}$$

Here, C_k $(k = 1, 2, \ldots, 6)$ are the linear combination coefficients, $\boldsymbol{x} = (x, y)$, and S_k and A_k $(k = 1, 2, 3)$ are defined by $S_k = C_k + C_{k+3}$ and $A_k = C_k - C_{k+3}$.

For a stress-free plate, there are three boundary conditions for the stress tensor σ

$$\sigma_{xz} = \sigma_{yz} = \sigma_{zz} = 0 \tag{16}$$

at each surface of the plate. Using Hooke's law and expressing the boundary conditions in terms of the lattice displacement, we obtain at $z = \pm\frac{1}{2}w$

$$\begin{cases} \dfrac{\partial u_x}{\partial z} + \dfrac{\partial u_z}{\partial x} = 0 \\ \dfrac{\partial u_y}{\partial z} + \dfrac{\partial u_z}{\partial y} = 0 \\ c_{12}\nabla \cdot \boldsymbol{u} + (2c_{44} + c^*)\dfrac{\partial u_z}{\partial z} = 0 \end{cases} \tag{17}$$

These boundary conditions can be satisfied independently for symmetric and antisymmetric modes with respect to the central plane of the plate.[39] Substitution of the symmetric part ($A_k = 0$) of Equation (14) and (15) into the boundary conditions gives

$$S\begin{bmatrix} S_1 \\ S_2 \\ S_3 \end{bmatrix} = 0 \tag{18}$$

and substitution of the antisymmetric part ($S_k = 0$) of Equation (14) and (15) into the boundary conditions gives

$$A\begin{bmatrix} A_1 \\ A_2 \\ A_3 \end{bmatrix} = 0 \tag{19}$$

Here, 3×3 matrices of S and A are defined by

$$\begin{cases} S_{1k} = \left(L_z^{(k)}\alpha_x^{(k)} + \ell_x\alpha_z^{(k)}\right)\sin\left(\frac{1}{2}qwL_z^{(k)}\right) \\ S_{2k} = \left(L_z^{(k)}\alpha_y^{(k)} + \ell_y\alpha_z^{(k)}\right)\sin\left(\frac{1}{2}qwL_z^{(k)}\right) \\ S_{3k} = \left[c_{12}(\ell_x\alpha_x^{(k)} + \ell_y\alpha_y^{(k)}) + c_{11}L_z^{(k)}\alpha_z^{(k)})\right] \times \cos\left(\frac{1}{2}qwL_z^{(k)}\right) \end{cases} \tag{20}$$

and

$$\begin{cases} A_{1k} = \left(L_z^{(k)}\alpha_x^{(k)} + \ell_x\alpha_z^{(k)}\right)\cos\left(\frac{1}{2}qwL_z^{(k)}\right) \\ A_{2k} = \left(L_z^{(k)}\alpha_y^{(k)} + \ell_y\alpha_z^{(k)}\right)\cos\left(\frac{1}{2}qwL_z^{(k)}\right) \\ A_{3k} = \left[c_{12}\left(\ell_x\alpha_x^{(k)} + \ell_y\alpha_y^{(k)}\right) + c_{11}\left(L_z^{(k)}\alpha_z^{(k)}\right)\right] \times \sin\left(\frac{1}{2}qwL_z^{(k)}\right) \end{cases} \tag{21}$$

where $k = 1, 2, 3$. For nontrivial solutions to Equation (18) (Equation (19)) to exist, the determinant of S (A) is required to vanish.

The numerical calculation of the vibrational modes can be done as follows. First, the magnitude q and the direction ϕ of the in-plane wavevector are determined. Under these conditions, the mode is obtained by scanning the frequencies ω to find the zeros of the determinant $|S|$ (for the symmetric modes) or $|A|$ (for the antisymmetric modes). The n-th zero, ω_n, of $|S|$ ($|A|$) found gives the dispersion curve of the n-th symmetric (antisymmetric) branch of the vibrational modes.

2.2. Interaction Potential

From Equation (14) and (15), the Fourier component of the lattice displacement vector $\boldsymbol{u}(\boldsymbol{q}, z)$ for the n-th symmetric branch is given by

$$u_{Sn}^j(\boldsymbol{q}, z) = \sum_{k=1}^{3} \beta_{Sn}^{j(k)} \cos(qL_z^{(k)}z), \quad (j = x, y) \tag{22}$$

$$u_{Sn}^z(\boldsymbol{q}, z) = \sum_{k=1}^{3} \beta_{Sn}^{z(k)} \sin(qL_z^{(k)}z) \tag{23}$$

and that for the n-th antisymmetric branch is given by

$$u_{An}^j(\boldsymbol{q}, z) = \sum_{k=1}^{3} \beta_{An}^{j(k)} \sin(qL_z^{(k)}z), \quad (j = x, y) \tag{24}$$

$$u_{An}^z(\boldsymbol{q}, z) = \sum_{k=1}^{3} \beta_{An}^{z(k)} \cos(qL_z^{(k)}z) \tag{25}$$

Here, $\beta_S^{j(k)}$ and $\beta_A^{j(k)}$ $(k = 1, 2, 3)$ are defined by

$$\beta_S^{j(k)} = \begin{cases} S_k\alpha_j^{(k)}, & (j = x, y) \\ i\,S_k\alpha_j^{(k)}, & (j = z) \end{cases} \tag{26}$$

and

$$\beta_{\mathrm{A}}^{j(k)} = \begin{cases} i A_k \alpha_j^{(k)}, & (j = x, y) \\ A_k \alpha_j^{(k)}, & (j = z) \end{cases} \tag{27}$$

The general displacement vector $\boldsymbol{u}(\boldsymbol{x})$ can be expressed in terms of phonon creation and annihilation operators $a_{\eta n \boldsymbol{q}}^{\dagger}$ and $a_{\eta n \boldsymbol{q}}$ as

$$\boldsymbol{u}(\boldsymbol{x}) = \sum_{\eta n \boldsymbol{q}} \left(\frac{\hbar}{2\rho S \omega_{\eta n \boldsymbol{q}}} \right)^{1/2} \boldsymbol{u}_{\eta n}(\boldsymbol{q}, z) \left(a_{\eta n \boldsymbol{q}} + a_{\eta n, -\boldsymbol{q}}^{\dagger} \right) \mathrm{e}^{i \boldsymbol{q} \cdot \boldsymbol{x}} \tag{28}$$

where η represents the symmetry of the mode ($\eta = S$ for symmetric and A for antisymmetric modes), S is the area, and $\boldsymbol{u}_{\eta n}(\boldsymbol{q}, z)$ is normalized as

$$\int_{-w/2}^{w/2} \boldsymbol{u}_{\eta n}^{\dagger}(\boldsymbol{q}, z) \cdot \boldsymbol{u}_{\eta n}(\boldsymbol{q}, z) \mathrm{d}z = 1 \tag{29}$$

We assume the following electron–acoustic-phonon interaction potential $U(\boldsymbol{x})$[30,42]

$$U(\boldsymbol{x}) = \sum_{ij} \Xi_{ij} \varepsilon_{ij}(\boldsymbol{x}) \tag{30}$$

Here, Ξ_{ij} $(i, j = x, y, z)$ is the deformation potential tensor, and $\varepsilon_{ij}(\boldsymbol{x})$ is the symmetrical strain tensor

$$\varepsilon_{ij}(\boldsymbol{x}) = \frac{1}{2} \left(\frac{\partial u_i}{\partial x_j} + \frac{\partial u_j}{\partial x_i} \right), \quad (i, j = x, y, z) \tag{31}$$

In this study, we consider the lowest electronic sub-band of the twofold valleys with the principal axis in the [001] direction (highlighted valleys in Figure 1b). In that case, the deformation potentials are written as[30]

$$\Xi = \begin{pmatrix} \Xi_{\mathrm{d}} & 0 & 0 \\ 0 & \Xi_{\mathrm{d}} & 0 \\ 0 & 0 & \Xi_{\mathrm{d}} + \Xi_{\mathrm{u}} \end{pmatrix} \tag{32}$$

where Ξ_{d} and Ξ_{u} are the dialational and shear deformation potential constants, respectively. Substitution of Equation (22–25) and (32) into Equation (30) gives

$$U(\boldsymbol{x}) = \sum_{\eta n \boldsymbol{q}} \left(\frac{\hbar}{2\rho S \omega_{\eta n \boldsymbol{q}}} \right)^{1/2} i C_{\eta n}(\boldsymbol{q}, z) \left(a_{\eta n \boldsymbol{q}} + a_{\eta n, -\boldsymbol{q}}^{\dagger} \right) e^{i \boldsymbol{q} \cdot \boldsymbol{x}} \tag{33}$$

where $C_{\eta n}(\boldsymbol{q}, z)$ is defined by

$$C_{\eta n}(\boldsymbol{q}, z) = \begin{cases} \sum_{k=1}^{3} X_{\eta n}^{(k)}(\phi) q \cos\left(q L_z^{(k)} z \right), & (\eta = S) \\ \sum_{k=1}^{3} X_{\eta n}^{(k)}(\phi) q \sin\left(q L_z^{(k)} z \right), & (\eta = A) \end{cases} \tag{34}$$

and $X_{\eta n}^{(k)}(\phi)$ (ϕ is the angle between $\boldsymbol{q}$ and the x-axis) is defined by

$$X_{\eta n}^{(k)}(\phi) = \begin{cases} \Xi_{\mathrm{d}} \left[\beta_{\eta n}^{x(k)} \ell_x + \beta_{\eta n}^{y(k)} \ell_y \right] \\ \quad - i[\Xi_{\mathrm{d}} + \Xi_{\mathrm{u}}] \beta_{\eta n}^{z(k)} L_z^{(k)}, & (\eta = S) \\ \Xi_{\mathrm{d}} \left[\beta_{\eta n}^{x(k)} \ell_x + \beta_{\eta n}^{y(k)} \ell_y \right] \\ \quad + i[\Xi_{\mathrm{d}} + \Xi_{\mathrm{u}}] \beta_{\eta n}^{z(k)} L_z^{(k)}, & (\eta = A) \end{cases} \tag{35}$$

2.3. Mobility

We first evaluate the intra-sub-band electron scattering rate for the lowest electronic sub-band of the twofold valleys. Let $\mathrm{e}^{i \boldsymbol{k} \cdot \boldsymbol{x}} \xi_0(z) / \sqrt{S}$ be the wavefunction of the ground sub-band and $E_0(\boldsymbol{k})$ $(= \hbar^2 k^2 / 2 m_{\mathrm{t}})$ be the in-plane energy dispersion. In the elastic equipartion energy approximation [11,13], the intra-ground-sub-band scattering rate, $S_{\boldsymbol{k} \to \boldsymbol{k}'}$, from an initial state $\boldsymbol{k}$ to a final state $\boldsymbol{k}'$ by absorption or emission of a phonon is given by

$$\begin{aligned} S_{\boldsymbol{k} \to \boldsymbol{k}'} &= f_{\nu} \frac{2\pi}{\hbar} \sum_{\eta n \boldsymbol{q}} \frac{kT}{\rho S \omega_{\eta n \boldsymbol{q}}^2} |\langle \xi_0(z) | C_{\eta n}(\boldsymbol{q}, z) | \xi_0(z) \rangle|^2 \\ &\quad \times \delta_{\boldsymbol{k}', \boldsymbol{k} + \boldsymbol{q}} \delta(E_0(\boldsymbol{k}') - E_0(\boldsymbol{k})) \\ &= f_{\nu} \frac{2\pi k T F_0}{\hbar \rho S v_{\ell}^2} \sum_{\boldsymbol{q}} \Xi_0^2(\boldsymbol{q}) \delta_{\boldsymbol{k}', \boldsymbol{k} + \boldsymbol{q}} \delta(E_0(\boldsymbol{k}') - E_0(\boldsymbol{k})) \end{aligned} \tag{36}$$

where f_{ν} is the valley degeneracy of the final state,[43] kT is the thermal energy, v_{ℓ} is the averaged longitudinal sound velocity in the isotropic approximation $v_{\ell} = (c_{\ell}/\rho)^{1/2}$ with $c_{\ell} = c_{12} + 2c_{44} + (3/5)c^*$,[44,45] and F_0 is the form factor

$$F_0 = \int_{-w/2}^{w/2} \xi_0^4(z) \, \mathrm{d}z \tag{37}$$

and $\Xi_0^2(\boldsymbol{q})$ is defined by

$$\Xi_0^2(\boldsymbol{q}) = \frac{1}{F_0} \sum_{\eta n} \frac{v_{\ell}^2}{\omega_{\eta n \boldsymbol{q}}^2} |\langle \xi_0(z) | C_{\eta n}(\boldsymbol{q}, z) | \xi_0(z) \rangle|^2 \tag{38}$$

For $\boldsymbol{q} = q(\cos\phi, \sin\phi)$, the ϕ dependence of $\Xi_0^2(\boldsymbol{q})$ is not large, so in the following we replace $\Xi_0^2(\boldsymbol{q})$ with the ϕ average of

$$\overline{\Xi_0^2}(q) = \frac{1}{2\pi} \int_0^{2\pi} \Xi_0^2(\boldsymbol{q}) \, \mathrm{d}\phi \tag{39}$$

Next we evaluate the momentum relaxation time τ_{α} to calculate the diagonal electron mobility $\mu_{\alpha\alpha}$ $(\alpha = x, y)$.[30] Since we are considering the electron mobility of the twofold valleys, the mobility is isotropic in the xy-plane and it is sufficient to calculate only τ_x. In the steady-state Boltzmann transport equation for a spatially homogeneous system, when the electron distribution function $f(\boldsymbol{k})$ is approximated by $f(\boldsymbol{k}) = f_0(k) + f_x(k)\omega_x + f_y(k)\omega_y$ with $|f_x|, |f_y| \ll f_0$ (f_0 is the distribution function at thermal equilibrium), the momentum relaxation time is given by

$$\frac{1}{\tau_x} = \frac{1}{\pi} \int_0^{\infty} \int_0^{2\pi} \int_0^{2\pi} \frac{S k' \mathrm{d}k' \mathrm{d}\varphi' \, \mathrm{d}\varphi}{(2\pi)^2} S_{\boldsymbol{k} \to \boldsymbol{k}'} \omega_x [\omega_x - \omega' x] \tag{40}$$

where $\boldsymbol{k} = (k_x, k_y) = k(\cos\varphi, \sin\varphi)$ and $\omega_\alpha = k_\alpha/k$ (the primed symbols are defined in the same way). Inserting Equation (36) into this equation, we have

$$\frac{1}{\tau_x} = f_\nu \frac{kTm_t F_0}{\hbar^3 \rho v_\ell^2} D_0^2(E_0(\boldsymbol{k})) \tag{41}$$

where the energy-dependent effective deformation potential constant, $D_0(E)$, for the intra-ground-sub-band scattering is given by

$$D_0^2(E_0(\boldsymbol{k})) = \frac{4}{\pi^2}\int_0^\pi \overline{\Xi}_0^2(2k\sin\theta)\theta\sin^2\theta\,\mathrm{d}\theta \tag{42}$$

As shown by Equation (41), the momentum relaxation time τ_x is a function of the initial electron energy E, $\tau_x(E)$.

We assume the nondegenerate electron gas whose thermal-equilibrium distribution function is $f_0(E) \propto \mathrm{e}^{-E/kT}$. The electron mobility μ_{xx} is then given by $\mu_{xx} = e\langle\tau_x\rangle/m_t$ with the averaged momentum relaxation time given by

$$\langle\tau_x\rangle = \int_0^\infty Ef_0(E)\tau_x(E)\,\mathrm{d}E \Big/ \int_0^\infty Ef_0(E)\,\mathrm{d}E \tag{43}$$

From Equation (41), we obtain

$$\langle\tau_x\rangle = \left[f_\nu \frac{kTm_t F_0}{\hbar^3\rho v_\ell^2}\right]^{-1} \frac{1}{(kT)^2}\int_0^\infty E\mathrm{e}^{-E/kT} D_0^{-2}(E)\,\mathrm{d}E \tag{44}$$

In the isotropic acoustic phonon approximation,[46] $\langle\tau_x\rangle$ is written as

$$\frac{1}{\langle\tau_x\rangle} = f_\nu \frac{kTm_t F_0 D_{\mathrm{ac}}^2}{\hbar^3\rho v_\ell^2} \tag{45}$$

Note that this Kawaji formula shows that the electron mobility is proportional to $(v_\ell/D_{\mathrm{ac}})^2$ and that the sound velocity as well as the deformation potential is an important factor in limiting the electron mobility. Comparing Equation (44) and (45), we can identify the effective deformation potential constant D_{ac} in the anisotropic model as

$$D_{\mathrm{ac}} = \left[\frac{1}{(kT)^2}\int_0^\infty E\mathrm{e}^{-E/kT} D_0^{-2}(E)\,\mathrm{d}E\right]^{-1/2} \tag{46}$$

3. Results and Discussion

3.1. Phonon Modes

We calculate the phonon modes using the following material parameters:[47] $c_{11} = 16.577 \times 10^{10}$ Pa, $c_{12} = 6.393 \times 10^{10}$ Pa, $c_{44} = 7.962 \times 10^{10}$ Pa, and $\rho = 232.9\,\mathrm{kg\,m^{-3}}$. **Figure 2** shows the sound velocities in the (001) plane of bulk Si as a function of angle ϕ from [100]. There are three modes, L, T1, and T2, which are the quasi-longitudinal, pure transverse, and quasi-transverse modes, respectively. For an isotropic model, the phonon modes are either pure longitudinal or pure transverse. For the anisotropic model, only the T1 mode is pure transverse. The other two modes, T2 and L, are not exactly transverse or longitudinal; the atoms vibrate perpendicular to or in the same direction as the wave propagation only in certain special crystal orientations. As a result, electrons can interact with both T2 and L modes. In the figure, we also plot the averaged longitudinal sound velocity, v_ℓ, and the averaged transverse sound velocity, v_t;[44,45] the latter is given by $v_t = (c_t/\rho)^{1/2}$ with $c_t = c_{44} + \frac{1}{5}c^*$. The present parameter set gives $v_\ell = 9.00\,\mathrm{km\,s^{-1}}$ and $v_t = 5.41\,\mathrm{km\,s^{-1}}$. As can be seen from the comparison with the isotropic model, the anisotropy in the Si crystal is not so large with the Zener anisotropy factor $A = 2c_{44}/(c_{11} - c_{12}) = 1.56$, but the sound velocity depends on the direction of the wave propagation.

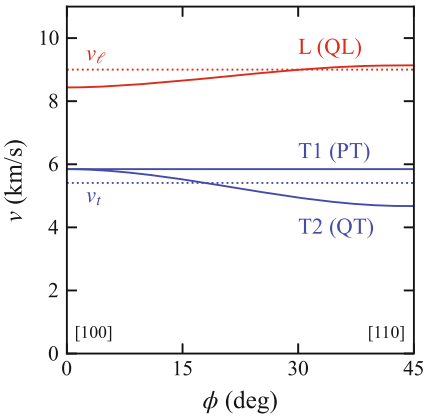

Figure 2. Sound velocities in the (001) plane of bulk Si as a function of angle ϕ from [100]. There are three modes, L, T1, and T2, which are the quasi-longitudinal, pure transverse, and quasi-transverse modes, respectively. Dotted lines show the averaged longitudinal and transverse velocities in the isotropic model.[44,45]

Figure 3 shows the dispersion relations of an anisotropic (001) Si plate, a) for the in-plane phonon wavevector, $\boldsymbol{q}$, along [100]; b) for 30° off the [100] axis; and c) for 45° off the [100] axis. For comparison, the dispersion relations of the longitudinal and transverse waves in bulk Si crystal are also plotted in the figure. **Figure 4** shows the dispersion relation of an isotropic Si plate whose elastic stiffness constants, $\hat{c}_{11}$, $\hat{c}_{12}$, and $\hat{c}_{44}$, are set to $\hat{c}_{11} = c_\ell$, $\hat{c}_{12} = c_\ell - 2c_t$, and $\hat{c}_{44} = c_t$ to give the Zener anisotropy factor $A = 1$ and the isotropic longitudinal and transverse velocities of v_ℓ and v_t. The dispersion relation in the anisotropic plate is found to depend on the direction of the wave propagation, similar to the angle dependence of the dispersion relation in the bulk. In addition, it is found to exhibit weakly oscillatory behavior, rather than the monotonic behavior of the isotropic plate. These characteristics can be understood through Mindlin's coupled mode theory[48] extended by Solie and Auld.[39] They relate the dispersions of a free-standing anisotropic plate to the uncoupled primary and shear vertical modes, which in turn are related to the slowness curves for bulk waves. This type of analysis provides a means of approximating the behavior of the dispersion curves from the behavior of the slowness curves and makes the dispersion curves understandable.[39]

3.2. Effective Deformation Potential

We consider an infinite quantum well model for the electronic states, where the wavefunction of the lowest sub-band, $\xi_0(z)$,

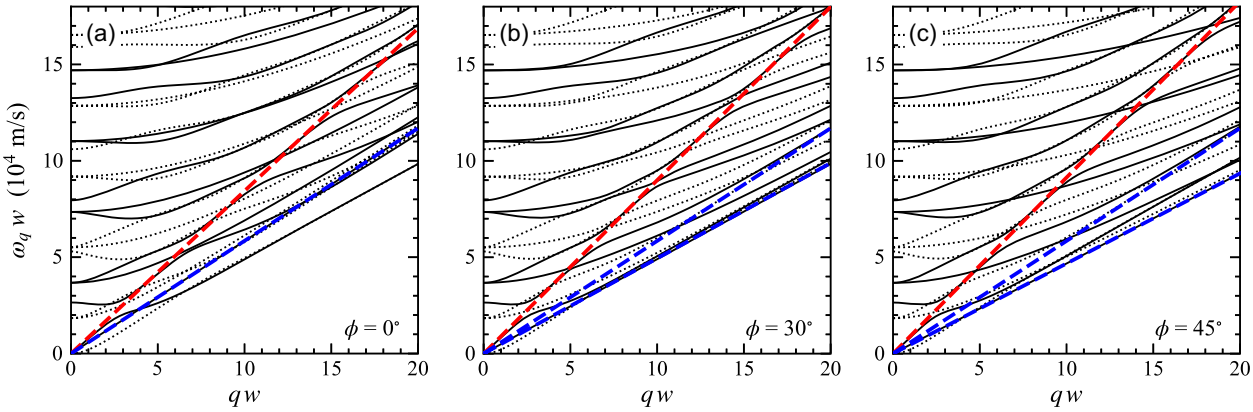

Figure 3. Dispersion relations of an anisotropic (001) Si plate, a) for the in-plane phonon wavevector, $\boldsymbol{q}$, along [100]; b) for 30° off the [100] axis; and c) for 45° off the [100] axis. Note that we plot $\omega_q w$ as a function of qw because the dispersion relation is scaled by the plate thickness w.[39] Black solid lines represent the symmetric and dotted lines the antisymmetric modes. For comparison, the bulk dispersion relations of (quasi-)longitudinal and (pure and quasi-)transverse waves are plotted by red and blue dashed lines, respectively.

associated with the quantized z-motion is given by

$$\xi_0(z) = \sqrt{\frac{2}{w}}\cos\left(\frac{\pi z}{w}\right), \quad \left(|z| < \frac{1}{2}w\right) \tag{47}$$

For this wavefunction, only the symmetric phonon modes interact with the electrons, and we have

$$\Xi_0^2(\boldsymbol{q}) = \frac{1}{F_0}\sum_n \frac{\nu_\ell^2 q^2}{\omega_{Snq}^2}\left|\sum_{k=1}^{3} X_{Sn}^{(k)}(\phi) G_0\left(\frac{1}{2}qwL_z^{(k)}\right)\right|^2 \tag{48}$$

where

$$G_0(x) = \frac{\sin x}{x[1-(x/\pi)^2]} \tag{49}$$

Figure 5 shows the effective deformation potential constant D_{ac} as a function of the plate thickness w at $T = 300$ K. The effective masses are set to $m_\ell = 0.916\, m_0$ and $m_t = 0.190\, m_0$,[11] and the deformation potential constants are $\Xi_d = 1.10$ eV and $\Xi_u = 10.5$ eV [49] Note that this parameter set of Ξ_d and Ξ_u gives the effective deformation potential D_{ac} of bulk Si as $D_{ac} = 10$ eV for the anisotropic model of Herring and Vogt (see Equation (54) and (55))[30] and 9.4 eV for the isotropic approximation using $\hat{c}_{11}$, $\hat{c}_{12}$, and $\hat{c}_{44}$.

The blue solid line shows $D_{ac}^{M,A}$ (the superscript M stands for modulated and A for anisotropic) for the modulated phonons in an anisotropic Si plate calculated with Equation (48). We see that $D_{ac}^{M,A}$ is almost constant ($D_{ac}^{M,A} \approx 13$ eV) in the thinner region of the plate thickness $w \lesssim 3.2$ nm. As the thickness increases $w \gtrsim 3.2$ nm, $D_{ac}^{M,A}$ decreases with w. This w-dependence can be explained as follows. In the thin plate limit, the electrons are strongly confined, so the effective 3D phonon wavevector[50] involved in the scattering is mainly oriented along the z-axis, leading to a larger deformation potential component involved (see Equation (32)). However, as the plate becomes thicker and the electrons are less confined, the effective phonon

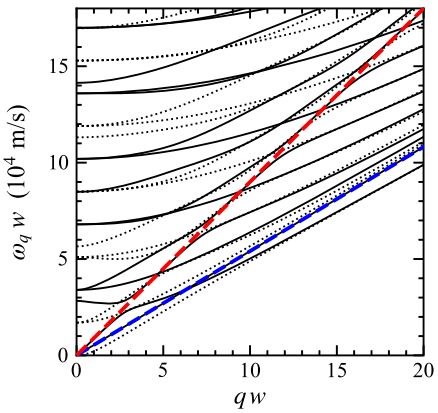

Figure 4. Dispersion relation of an isotropic Si plate. Black solid lines represent the symmetric and dotted lines the antisymmetric modes. Red and blue dashed lines show $\omega_q = \nu_\ell q$ and $\nu_t q$, respectively.

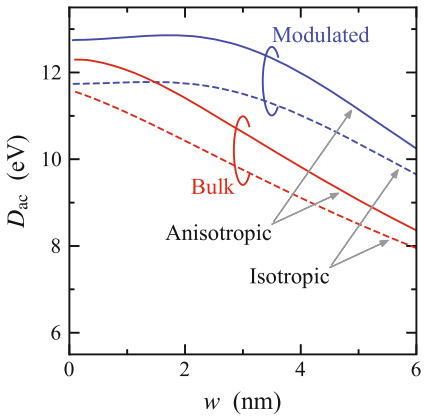

Figure 5. The effective deformation potential constant D_{ac} as a function of the plate thickness w at $T = 300$ K. Blue solid (dashed) line shows $D_{ac}^{M,A}$ ($D_{ac}^{M,I}$) for the modulated phonons in the anisotropic model (isotropic approximation), and red solid (dashed) line shows $D_{ac}^{B,A}$ ($D_{ac}^{B,I}$) for the bulk phonons in the anisotropic model (isotropic approximation).

wavevector will tilt toward the xy plane, thus weakening the deformation potential component involved in the scattering.

Note that in the present study, we consider only the lowest sub-band and neglect higher sub-bands, which should be considered for thicker w region; the decrease in D_{ac} as a function of w shown in Figure 5 does not necessarily imply an increase in the total mobility with the higher sub-bands contributions.

In Figure 5, we also plot $D_{ac}^{M,I}$ for the modulated phonons in the isotropic approximation using $\hat{c}_{11}$, $\hat{c}_{12}$, and $\hat{c}_{44}$ by the blue dashed line, showing a similar w-dependence to $D_{ac}^{M,A}$, but with smaller values. For example, $D_{ac}^{M,I} = 11.8$eV and $D_{ac}^{M,A} = 12.8$ eV at $w = 1$ nm. This smaller $D_{ac}^{M,I}$ than $D_{ac}^{M,A}$ is mainly due to the smaller sound velocity in the anisotropic model. As shown in Figure 3, the lowest symmetric mode at around $q = 0$ almost follows the bulk quasi-longitudinal mode, and the quasi-longitudinal sound velocity in bulk Si for the [100] direction, $v_{[100]} = 8.44\,\mathrm{km\,s^{-1}}$ (see Figure 2), is smaller than the averaged longitudinal sound velocity $v_\ell = 9.00\,\mathrm{km\,s^{-1}}$. For thin plates, the contribution of phonons oriented along the z-axis is considered large. We thus estimate the deformation potential ratio $D_{ac}^{M,I}/D_{ac}^{M,A}$ by the square of the velocity ratio $(v_{[100]}/v_\ell)^2$ (= 0.88), which is almost equal to and slightly smaller than $D_{ac}^{M,I}/D_{ac}^{M,A}$ (= 0.92 at $w = 1$ nm).

In Figure 5, the red solid (dashed) line shows $D_{ac}^{B,A}$ ($D_{ac}^{B,I}$) for the bulk phonons in the anisotropic model (isotropic approximation). In the bulk phonon model, $\Xi_0^2(q)$ is given by

$$\Xi_0^2(q) = \frac{1}{F_0}\int_0^{2\pi}\frac{\mathrm{d}\,q_z}{2\pi}\left[\Xi_\ell^2(\theta) + \frac{v_\ell^2}{v_t^2}\,\Xi_t^2(\theta)\right] G_0^2\left(\frac{1}{2}qw\right) \tag{50}$$

Here, θ is the angle between the 2D phonon wavevector $\boldsymbol{q}$ and q_z, and $\Xi_\ell^2(\theta)$ and $\Xi_t^2(\theta)$ are defined by

$$\Xi_\ell^2(\theta) = (\Xi_\mathrm{d} + \Xi_\mathrm{u}\cos^2\theta)^2 f_\ell(\theta) \tag{51}$$

$$\Xi_\mathrm{t}^2(\theta) = \Xi_\mathrm{u}^2\cos^2\theta\sin^2\theta f_\mathrm{t}(\theta) \tag{52}$$

and

$$f_\ell(\theta) = f_\mathrm{t}(\theta) = 1 \tag{53}$$

for the isotropic approximation and

$$f_\ell(\theta) = 1 - \frac{c^*(0.15 - 1.50\cos^2\theta + 1.75\cos^4\theta)}{c_\ell} \tag{54}$$

$$f_\mathrm{t}(\theta) = c_\mathrm{t}\left[\frac{3}{c_{44}+\frac{1}{3}c^*} - \frac{2}{c_{44}+\frac{1}{2}c^*} + 6\cos^2\theta\left[\frac{1}{c_{44}+\frac{1}{2}c^*} - \frac{1}{c_{44}+\frac{1}{3}c^*}\right]\right] \tag{55}$$

for the anisotropic model of Herring and Vogt.[30] Comparing the results between the modulated phonons ($D_{ac}^{M,A}$ and $D_{ac}^{M,I}$) and the bulk phonons ($D_{ac}^{B,A}$ and $D_{ac}^{B,I}$), we can see that not only the crystal anisotropy but also the phonon modulation have non-negligible effects on the effective deformation potential and the electron mobility.

4. Conclusion

We have studied the electron–acoustic-phonon interaction in a free-standing Si plate with (001) surface, taking into account the elastic anisotropy of the Si crystal and the modulated phonon modes obtained by the calculation method of Solie and Auld.[39] Using the obtained phonon modes, we derived the electron–acoustic-phonon interaction potential with the anisotropic deformation potential constants. Considering only the lowest electronic sub-band, we calculated the electron mobility and converted it to the effective deformation potential constant D_{ac}.

The dispersion relation in the anisotropic plate is found to depend on the direction of the wave propagation, similar to the angle dependence of the bulk dispersion relation. In addition, it is found to exhibit weakly oscillatory behavior, rather than the monotonic behavior of the isotropic plate, as explained by the extended coupled-mode theory.[39,48]

In the quantum well model for the electronic states, we find that the effective deformation potential, $D_{ac}^{M,A}$, for the modulated phonons in an anisotropic Si plate becomes $D_{ac}^{M,A} \approx 13$ eV in the thinner region of the plate thickness $w \lesssim 3.2$ nm. The effect of the elastic anisotropy on the effective deformation potential is found to be rather large; for example, it is reduced by ≈1 eV in the thinner region if we assume the isotropic approximation. We also find that the phonon modulation and the crystal anisotropy have non-negligible effects on the effective deformation potential and the electron mobility. Note that only the lowest sub-band is considered in this study, so the calculations must take into account the excited sub-bands and the upper valleys for consideration in the thicker plate region. Such studies are the subject of future work.

Physically reliable modeling is essential for the realization of ultrasmall Si MOS transistors. As shown in this study, the conventional isotropic model using a constant deformation potential is insufficient for modeling acoustic phonon scattering in confined structures. The method presented in this paper is applicable to device modeling of 2D structures such as SOI MOSFETs. In the case of 3D structures such as nanosheets, the phonons are confined in 2D, so the method in this paper is not directly applicable, but can be extended. In both cases, the actual design of transistors requires simplified modeling that can be implemented in technology computer-aided design tools. For this purpose, the effective deformation potential D_{ac} should be the key parameter. However, as shown in this study, the effective deformation potential varies with the plate thickness. Also, although not included in this paper, numerical tests show that the effective deformation potential is also affected by the shape of the wavefunctions and the excited sub-bands (valleys). Therefore, it may not be possible to analyze the electron transport properties in confined channel devices using only a single constant of D_{ac}.

Acknowledgements

The author thanks Dr. Hajime Tanaka for helpful discussions. This work was supported by JSPS KAKENHI grant no. JP20H00250.

Conflict of Interest

The author declares no conflict of interest.

Data Availability Statement

The data that support the findings of this study are available from the corresponding author upon reasonable request.

Keywords

electron transport, electron–phonon interactions, electrons, phonons, silicon

Received: October 15, 2024
Revised: November 28, 2024
Published online:

[1] N. Loubet, T. Hook, P. Montanini, C.-W. Yeung, S. Kanakasabapathy, M. Guillom, T. Yamashita, J. Zhang, X. Miao, J. Wang, A. Young, R. Chao, M. Kang, Z. Liu, S. Fan, B. Hamieh, S. Sieg, Y. Mignot, W. Xu, S.-C. Seo, J. Yoo, S. Mochizuki, M. Sankarapandian, O. Kwon, A. Carr, A. Greene, Y. Park, J. Frougier, R. Galatage, R. Bao, et al., in *2017 Symp. on VLSI Technology*. Kyoto, June **2017**, pp. T230–T231.
[2] G. Bae, D.-I. Bae, M. Kang, S. Hwang, S. Kim, B. Seo, T. Kwon, T. Lee, C. Moon, Y. Choi, K. Oikawa, S. Masuoka, K. Chun, S. Park, H. Shin, J. Kim, K. Bhuwalka, D. Kim, W. Kim, J. Yoo, H. Jeon, M. Yang, S.-J. Chung, D. Kim, B. Ham, K. Park, W. Kim, S. Park, G. Song, Y. Kim, et al., in *2018 IEEE Int. Electron Devices Meeting (IEDM)* San Francisco, December **2018**, pp. 28.7.1–28.7.4.
[3] J. Zhang, J. Frougier, A. Greene, X. Miao, L. Yu, R. Vega, P. Montanini, C. Durfee, A. Gaul, S. Pancharatnam, C. Adams, H. Wu, H. Zhou, T. Shen, R. Xie, M. Sankarapandian, J. Wang, K. Watanabe, R. Bao, X. Liu, C. Park, H. Shobha, P. Joseph, D. Kong, A. A. De La Pena, J. Li, R. Conti, D. Dechene, N. Loubet, R. Chao, et al., in *2019 IEEE Int. Electron Devices Meeting (IEDM)* San Francisco, December **2019**, pp. 11.6.1–11.6.4.
[4] S. Mochizuki, M. Bhuiyan, H. Zhou, J. Zhang, E. Stuckert, J. Li, K. Zhao, M. Wang, V. Basker, N. Loubet, D. Guo, B. Haran, H. Bu, in *2020 IEEE Int. Electron Devices Meeting (IEDM)* Virtual Conference, December **2020**, pp. 2.3.1–2.3.4.
[5] S. Kim, K. Lee, S. Kim, M. Kim, J.-H. Lee, S. Kim, B.-G. Park, *IEEE Trans. Electron Devices* **2022**, *69*, 2088.
[6] N. Loubet, C. Durfee, J. Frougier, S. Mochizuki, M. Bhuiyan, R. Bao, A. Greene, E. Miller, I. Seshadri, in *Extended Abstracts of the 2021 Int. Conf. on Solid State Devices and Materials (SSDM)* Virtual Conference, September **2023**, pp. 63–64.
[7] S. Mochizuki, N. Loubet, P. Mirdha, C. Durfee, H. Zhou, G. Tsusui, J. Frougier, R. Vega, L. Qin, N. Felix, D. Guo, H. Bu, in *2023 Int. Electron Devices Meeting (IEDM)* San Francisco, December **2023**, pp. 1–4.
[8] R.-H. Yan, A. Ourmazd, K. Lee, *IEEE Trans. Electron Devices* **1992**, *39*, 1704.
[9] T. Ando, A. Fowler, F. Stern, *Rev. Mod. Phys.* **1982**, *54*, 437.
[10] C. Jacoboni, L. Reggiani, *Rev. Mod. Phys.* **1983**, *55*, 645.
[11] M. Lundstrom, *Fundamentals of Carrier Transport*, 2nd ed., Cambridge University Press, Cambridge **2000**.
[12] C. Jacoboni, *Theory of Electron Transport in Semiconductors*, Springer-Verlag, Berlin **2010**.
[13] D. Esseni, P. Palestri, L. Selmi, *Nanoscale MOS Transistors*, Cambridge University Press, Cambridge **2011**.
[14] M. V. Fischetti, W. G. Vandenberghe, *Advanced Physics of Electron Transport in Semiconductors and Nanostructures*, Springer International Publishing, Switzerland **2016**.
[15] C. Hamaguchi, *Basic Semiconductor Physics*, 4th ed., Springer Nature, Switzerland **2023**.
[16] H. Ezawa, S. Kawaji, K. Nakamura, *Surf. Sci.* **1971**, *27*, 218.
[17] H. Ezawa, T. Kuroda, K. Nakamura, *Surf. Sci.* **1971**, *24*, 654.
[18] H. Ezawa, S. Kawaji, T. Kuroda, K. Nakamura, *Surf. Sci.* **1971**, *24*, 659.
[19] H. Ezawa, *Ann. Phys.* **1971**, *67*, 438.
[20] H. Ezawa, S. Kawaji, K. Nakamura, *Jpn. J. Appl. Phys.* **1974**, *13*, 126.
[21] N. Bannov, V. Mitin, M. Stroscio, *Phys. Status Solidi B* **1994**, *183*, 131.
[22] N. Bannov, V. Aristov, V. Mitin, M. Stroscio, *Phys. Rev. B* **1995**, *51*, 9930.
[23] N. Bannov, V. Aristov, V. Mitin, *J. Appl. Phys.* **1995**, *78*, 5503.
[24] L. Donetti, F. Gamiz, J. B. Roldan, A. Godoy, *J. Appl. Phys.* **2006**, *100*, 013701.
[25] L. Donetti, F. Gamiz, J. B. Roldan, A. Godoy, *J. Comput. Electron.* **2006**, *5*, SI 199.
[26] S. Uno, N. Mori, *Jpn. J. Appl. Phys.* **2007**, *46*, L923.
[27] S. Uno, D. Yong, N. Mori, *Phys. Rev. B* **2009**, *79*, 23.
[28] S. Uno, J. Hattori, K. Nakazato, N. Mori, *Math. Comput. Modell.* **2010**, *51*, 863.
[29] S. Uno, J. Hattori, K. Nakazato, N. Mori, *J. Comput. Electron.* **2011**, *10*, 104.
[30] C. Herring, E. Vogt, *Phys. Rev.* **1956**, *101*, 944.
[31] E. M. Conwell, *High Field Transport in Semiconductors*, Solid State Physics, Supplement 9. Academic Press, New York, NY **1967**.
[32] C. Canali, C. Jacoboni, F. Nava, G. Ottaviani, A. Alberigiquaranta, *Phys. Rev. B* **1975**, *12*, 2265.
[33] R. Brunetti, C. Jacoboni, F. Nava, L. Reggiani, G. Bosman, R. Zijlstra, *J. Appl. Phys.* **1981**, *52*, 6713.
[34] K. Masaki, C. Hamaguchi, K. Taniguchi, M. Iwase, *Jpn. J. Appl. Phys.* **1989**, *28*, 1856.
[35] C. Jungemann, A. Emunds, W. Engl, *Solid-State Electron.* **1993**, *36*, 1529.
[36] S. Takagi, A. Toriumi, M. Iwase, H. Tango, *IEEE Trans. Electron Devices* **1994**, *41*, 2363.
[37] S. Takagi, J. Hoyt, J. Welser, J. Gibbons, *J. Appl. Phys.* **1996**, *80*, 1567.
[38] T. Ohashi, T. Tanaka, T. Takahashi, S. Oda, K. Uchida, *IEEE J. Electron Devices Soc.* **2016**, *4*, 278.
[39] L. Solie, B. Auld, *J. Acoust. Soc. Am.* **1973**, *54*, 50.
[40] J. F. Nye, *Physical Properties of Crystals*, Oxford Universality Press, Oxford **1957**.
[41] B. Auld, *IEEE Trans. Microwave Theory Tech.* **1969**, *17*, 800.
[42] P. Y. Yu, M. Cardona, *Fundamentals of Semiconductors*, 4th ed., Springer, Heidelberg **2010**.
[43] The effective deformation constant defined in this study is independent of the value of f_v, although $f_v = 1$ or $f_v = 2$ have been reported in the literature.
[44] F. I. Fedorov, *Theory of Elastic Waves in Crystals*, Prenum Press, New York, NY **1968**.
[45] Y. Sirenko, K. Kim, M. Stroscio, *Phys. Rev. B* **1997**, *56*, 15770.
[46] S. Kawaji, *J. Phys. Soc. Jpn.* **1969**, *27*, 906.
[47] O. Madelung, *Semiconductors: Data Handbook*, 3rd ed., Springer-Verlag, Berlin **2003**.
[48] R. D. Mindlin, in *Structural Mechanics* (Eds: J. N. Goodier, N. J. Hoff), Pergamon Press, Oxford **1960**, pp. 199–232.
[49] M. Fischetti, S. Laux, *J. Appl. Phys.* **1996**, *80*, 2234.
[50] See the discussion on pp. 185–186 of Reference [13].